

Position and Orientation Control of Remotely Operated Vehicles Utilizing Radial Basis Function Neural Networks to Overcome Underwater Environmental Disturbances

Hendi Purnata

Department of Electro and Mechatronic Engineering, Politeknik Negeri Cilacap, Cilacap, Indonesia |
Doctoral Program in Engineering, Universitas Negeri Yogyakarta, Yogyakarta, Indonesia
hendipurnata.2024@student.uny.ac.id

Moh. Khairudin

Department of Electrical Engineering, Universitas Negeri Yogyakarta, Yogyakarta, Indonesia
moh_khairudin@uny.ac.id (corresponding author)

Sarwo Pranoto

Department of Electrical Engineering, Universitas Negeri Yogyakarta, Yogyakarta, Indonesia
sarwopranoto@uny.ac.id

Galih Mustiko Aji

Department of Electro and Mechatronic Engineering, Politeknik Negeri Cilacap, Cilacap, Indonesia
galihma@gmail.com

Nanda Pranandita

Department of Mechanical Engineering, Politeknik Manufaktur Bangka Belitung, Bangka Belitung, Indonesia
nda.akano@gmail.com

Received: 19 September 2025 | Revised: 31 October 2025 | Accepted: 6 November 2025

Licensed under a CC-BY 4.0 license | Copyright (c) by the authors | DOI: <https://doi.org/10.48084/etasr.14930>

ABSTRACT

Conventional control systems, such as Proportional Integral Derivative (PID), have difficulty adapting to changes, which reduces the stability and efficiency of Remotely Operated Vehicles (ROVs). This study develops an adaptive control system based on Radial Basis Function Neural Network (RBFNN) combined with PID to improve PID adjustment and ROV stability. The research methodology involves designing RBFNN and PID controls, simulating them in MATLAB/Simulink, and testing them in three scenarios: calm currents, strong currents, and random disturbances. The uniqueness of this study lies in how it overcomes existing challenges and offers a new approach to ROV control in dynamic environments by comparing 6- and 8-thruster configurations on ROVs. The simulation results show that the application of RBFNN successfully reduces oscillations in the X position (0–2.5 m), Y position (-1 m), Z position (vertical drift), Roll, Pitch, and Yaw orientations. After RBFNN control, the ROV's position and orientation become more stable and closer to the setpoint, with an error of less than 1%. This study shows that MK-RBFNN-based adaptive control with an 8-thruster configuration can improve the stability and responsiveness of ROVs in dynamic environmental conditions. The significance of this research lies in the challenge of controlling ROVs for underwater structure inspection in dynamic environmental conditions.

Keywords-remotely operated vehicle; Radial Basis Function Neural Network (RBFNN); adaptive control system; underwater environment

I. INTRODUCTION

Inspection and maintenance of underwater structures, such as dams, bridges, offshore platforms, and pipeline networks, are crucial activities to ensure the integrity and safety of these facilities [10]. Traditionally, these tasks were performed by human divers, but technological advances now enable the use of robotic solutions that can improve safety and efficiency [11]. ROVs and Autonomous Underwater Vehicles (AUVs) have emerged as the primary solutions in this sector, offering numerous advantages in terms of reducing risk to humans and increasing operational duration and range in underwater environments [12].

ROVs have been widely used for inspection, maintenance, and repair tasks in the oil and gas industry, offshore platforms, and submerged pipelines [13]. The former can perform structural inspections and maintenance efficiently and with a lower level of risk compared to traditional methods [14]. However, the underwater environment is filled with factors, such as currents, waves, pressure, and resistance, which significantly affect the stability and control of ROVs [15, 16].

Variable currents in speed and direction can make it difficult for ROVs to maintain a stable position, with high current speeds requiring ROVs to have greater thrust capabilities to counteract these forces [17]. Wave action can cause dynamic movement in ROVs, exacerbating control and stability issues. Increased hydrostatic pressure at greater depths can affect ROV structural integrity. Moreover, the drag or resistance experienced by ROVs affects their maneuverability [18].

Although ROVs show great potential, there are still challenges in improving their autonomy and reliability owing to environmental constraints and the infrastructure costs required to support underwater robot systems [1, 2]. Continuous research and development are essential to overcome challenges such as predictive and system modeling [3, 4]. However, conventional control systems, such as PID, are insufficient to overcome these challenges. An adaptive control system based on RBFNN, instead, has the potential to provide a more effective solution in improving the underwater stability and maneuverability of ROVs [5, 6]. RBFNN can adjust control in real-time, providing stability and efficiency despite external disturbances [7, 8]. The specific problem faced is determining how the number and arrangement of thrusters, particularly the comparison between 6 and 8 thruster configurations, affects ROV performance metrics such as position and orientation accuracy, energy consumption, and tolerance to errors [9].

RBFNN is used to create a reference model that represents the dynamics of nonlinear systems, which is important for adaptive control [19, 20]. The reference model can be designed to change dynamically, allowing real-time adjustments to the control strategy [21, 22]. As a further application, the use of multi-kernel RBFNN enhances adaptive learning, providing better performance in dynamic nonlinear systems [23]. RBFNN-based adaptive PID control methods can identify controlled plants online and adjust PID controllers as needed.

Thus, this study addresses the challenges faced by ROV control systems in extreme underwater conditions by developing an adaptive control system based on RBFNN, which is more responsive to changes in environmental conditions. The application of this system is expected to not only improve the stability and accuracy of ROV maneuvers but also provide a more efficient and safer solution compared to conventional inspection methods. This research is expected to make a real contribution to the development of ROV technology for the inspection and maintenance of underwater structures, as well as empower local communities to adapt to challenging environments.

II. METHODOLOGY

The current study develops an RBFNN-based adaptive control system to improve ROV performance in dynamic underwater environments.

A. Basic ROV Dynamics

ROV dynamics [18] refer to the former's movement behavior in response to forces and moments acting on it in a three-dimensional underwater environment. This system is typically modeled in six Degrees of Freedom (6 DoFs), including three linear translations (surge, sway, heave) and three rotations (roll, pitch, yaw). Figure 1 shows the ROV reference frame for movement in 6 DoFs.

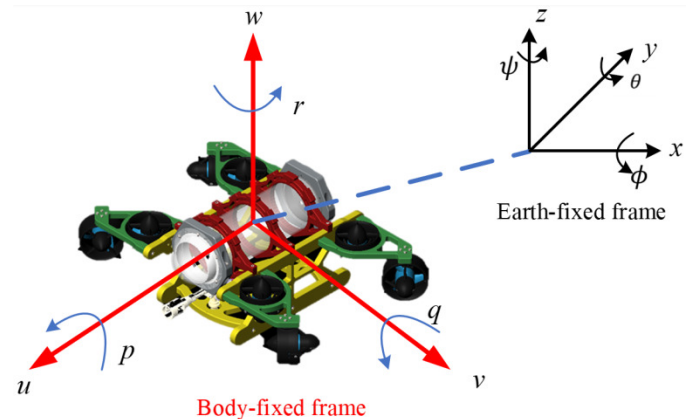


Fig. 1. Body fixed frame and earth fixed frame.

Figure 1 displays the body and earth frames, with position and orientation defined in the earth fixed frame at (1). Additionally, the linear velocity and angular velocity of the ROV are presented in body fixed frame notation at (2). The diagram also incorporates the configuration of 8 thrusters, which consists of 4 horizontal thrusters (T_1 – T_4) and 4 diagonal thrusters (T_5 – T_8). The body-fixed frame and the additional diagonal thrusters contribute significantly to the enhanced stability and maneuverability of the ROV, especially in controlling roll, pitch, and yaw orientations. The placement of these thrusters, especially the diagonal ones, improves the overall system's response to dynamic environmental conditions, making it more stable and efficient in maintaining position and orientation compared to the traditional 6-thruster configuration.

$$\eta = [x \quad y \quad z \quad \phi \quad \theta \quad \psi] \quad (1)$$

$$v = [v \ w]^T = [u \ v \ w \ p \ q \ r]^2 \quad (2)$$

Velocity in the Earth-fixed frame can be obtained from the ROV's velocity in the body-fixed frame by:

$$\dot{\eta} = J(\eta)v = \begin{bmatrix} R(\eta) & 0 \\ 0 & T(\eta) \end{bmatrix} \quad (3)$$

Ignoring disturbances, such as waves and tether, the dynamics of the ROV can be expressed as:

$$M\dot{v} + C(v)v + D(v)v + g(\eta) = \tau \quad (4)$$

where:

$$M = M_{RB} + M_A \quad (5)$$

$$C = C_{RB} + C_A \quad (6)$$

$$M_{RB} = \begin{bmatrix} mI_3 & -m[r_g]_x \\ m[r_g]_x & I \end{bmatrix} \quad (7)$$

$$M_A = -diag(\dot{X}_u, \dot{Y}_v, \dot{Z}_w, \dot{K}_p, \dot{M}_q, \dot{N}_r) \quad (8)$$

Equation (4), which consists of mass ($C(v)v$) or Coriolis and centripetal forces ($D(v)v$), damping forces ($g(\eta)$), and hydrostatic forces ($\tau = [X \ Y \ Z \ K \ M \ N]$), shows the total propulsion force vector in 6 DoFs. The Coriolis rigid body can be seen in:

$$C_{RB} = \begin{bmatrix} 0 & -m[v]_x \\ -m[v]_x & -[I\omega]_x \end{bmatrix} \quad (9)$$

$C_A(v)$ built consistently from M_A

$$D(v) = D_l + D_q(v)$$

$$D_l = diag(X_u, Y_v, Z_w, K_p, M_q, N_r)$$

$$D_q(v) = diag(q \odot |v|) \quad (10)$$

with $q = [X_{uu}, Y_{vv}, Z_{ww}, K_{pp}, M_{qq}, N_{rr}]^T$, and

$$g(\eta) =$$

$$\begin{bmatrix} (W - B) \sin \epsilon \\ -(W - B) \cos \epsilon \sin \phi \\ -(W - B) \cos \epsilon \cos \phi \\ -(y_g W - y_b B) \cos \epsilon \cos \phi + (z_g W - z_b B) \cos \epsilon \sin \phi \\ (z_g W - z_b B) \sin \epsilon + (x_g W - x_b B) \cos \epsilon \cos \phi \\ -(x_g W - x_b B) \cos \epsilon \sin \phi - (y_g W - y_b B) \sin \epsilon \end{bmatrix} \quad (11)$$

The ROV can become buoyancy neutral according to (11), which balances gravity and buoyancy with $W = B$. Additional mass is placed on the ROV to make the X-Y coordinates of CB coincide with the X-Y coordinates of CG ($x_G = x_B = 0, y_G = y_B = 0$). The resulting vector is:

$$G(\eta) = \begin{bmatrix} 0 \\ 0 \\ 0 \\ (z_G - z_B)W \ c_\theta s_\phi \\ (z_G - z_B)W \ s_\phi \\ 0 \end{bmatrix} \quad (12)$$

Control using an octarotor having 8 actuators, following the equation:

$$\tau = \sum_{i=1}^8 \begin{bmatrix} d_i \\ r_i \times d_i \end{bmatrix} u_i = Tu$$

$$T = \begin{bmatrix} d_1 & \dots & d_8 \\ r_1 \times d_1 & \dots & r_1 \times d_1 \end{bmatrix} \quad (13)$$

Then, the final ROV model becomes:

$$\dot{\eta} = J(\eta)v \quad (14)$$

$$v = M^{-1}(Tu_{sat} - C(v)v - D(v)v - g(\eta)) \quad (15)$$

B. Configuration Thruster

The thruster configuration matrix is arranged based on the position (x, y, z) and direction of the force generated by each thruster relative to the ROV's center of mass. This matrix serves to calculate the contribution of force and torque from each thruster to the ROV system. Force allocation analysis is performed using the pseudo-inverse, which considers the physical limitations of thruster force. This thruster configuration is then compared between the use of 6 and 8 thrusters, which is used as the basis for the RBFNN adaptive control system.

C. Adaptive Control Based on RBFNNs

To implement adaptive control based on RBFNNs [24], (16) can be followed by taking the network input vector:

$$z = \begin{bmatrix} e_\eta \\ e_v \end{bmatrix} \in \mathbb{R}^{12} \quad (16)$$

Then, using the Gaussian activation kernel from m kernel for data z , where σ controls the width of the Gaussian kernel function and c_i is the kernel center, which is written as:

$$\phi(z) = \begin{bmatrix} \exp\left(-\frac{\|z-c_1\|^2}{2\sigma^2}\right) \\ \vdots \\ \exp\left(-\frac{\|z-c_m\|^2}{2\sigma^2}\right) \\ 1 \end{bmatrix} \in \mathbb{R}^{m+1} \quad (17)$$

Equation (17) represents the Gaussian activation to the kernel plus bias. Then, the NN output equation is mapped to the moment:

$$\tau_{NN} = W\phi(z), \quad W \in \mathbb{R}^{6 \times (m+1)} \quad (18)$$

The shear surface is calculated as:

$$s = e_\eta + \Lambda e_v \quad (19)$$

$$\Lambda = diag(\lambda_1, \dots, \lambda_6) > 0 \quad (20)$$

The robust part is given by:

$$\tau_{robust} = K_r \tanh\left(\frac{s}{\delta}\right) \quad (21)$$

where $K_r = diag(k_{r,i}) > 0$ and $\delta > 0$ is referred to as the boundary layer. Gradient adjustment for weight adaptation is performed with projection to limit the weight:

$$\dot{W} = \Gamma s \phi(z)^T - \Pi_W(W) \quad (22)$$

$$\Gamma = diag(\gamma_1, \dots, \gamma_6) > 0$$

where Π_W is the projection operator (e.g., row scaling of W_i , when $\|W_i\| > W_{max}$). In discrete implementation:

$$W(k + 1) = W(k) + \dot{W} \Delta t \tag{23}$$

Stability with the Lyapunov function was used as:

$$V = \frac{1}{2} s^T M s + \sum_{i=1}^6 \frac{1}{2\gamma_i} \|W_i - W_i^*\|^2, \tag{24}$$

where W^* is the ideal weight that approximates the residual uncertainty.

Using the dynamics, $M\dot{v} = \tau - C v - D v - g$, the definition of s as the antisymmetry property $M - 2C$, and ignoring small approximation terms, the following relation is obtained:

$$V \leq -s^T D v - \sum_i k_{r,i} |\tanh(s_i / \delta) s_i| + (\text{approximation limit } NN). \tag{25}$$

With sufficiently large choices of $k_{r,i}$ and adequate adaptation rate γ_i ,

$$\dot{V} \leq -\alpha \|s\|^2 + \epsilon$$

Thus, s is bounded, and with the sliding surface property, the tracking error e_η, e_v is ultimately bounded. The weight projection ensures that W is bounded, thus not corrupting the analysis. Therefore, to determine the target force τ , it is translated into an actuator command:

$$u^* = T^\dagger \tau (\text{pseudoinvers SVD}) \tag{26}$$

$$u_{sat} = \min(\max(u^*, u_{min}), u_{max}) \tag{27}$$

If desired, constrained quadratic minimization can be used to manage saturation and DoF priority weights. In this implementation, per-actuator saturation is applied component-by-component before calculating $\tau = T u_{sat}$.

III. RESULTS AND DISCUSSION

This study analyzes the actuator and the linearized model response to produce a linear system that is easier to analyze. The control system is also applied to evaluate the control performance on the developed model. Based on Figure 1, the parameters used are adjusted to the requirements of the ROV, as listed in Table I.

Table I shows the parameters that are controlled through Simulink/MATLAB simulation. The actuator has six DoFs: translation along the X, Y, and Z axes, and rotation in roll, pitch, and yaw. The transformation matrix T is used to maintain the stability and position of the ROV according to the desired coordinates. Equation (11) controls the eight motors to stabilize the ROV, resulting in thruster control. The saturation function u_{sat} ensures that the input does not exceed the limits, with torque τ calculated using matrix T , which connects the thruster input with the torque on the X, Y, Z axes, as well as the roll (ϕ), pitch (θ), and yaw (ψ) orientations.

The configuration matrix for the six thrusters describes the relationship between the forces and moments generated by the ROV, with four horizontal thrusters (T₁–T₄) controlling surge, sway, and yaw, while two vertical thrusters (T₅–T₆) control heave and pitch. The configuration matrix for 6 thrusters is

designed to achieve maneuverability and ROV control stability, while maintaining full control over 6 DoFs [25].

TABLE I. CONTROL PARAMETERS

Parameter	Symbol	Value	Unit
Mass	m	40.000	kg
Mass moment	I_{xx}	45.333	kg·m ²
	I_{yy}	6.000	
	I_{zz}	8.133	
Weight	W	392.4	N
Buoyancy	B	615.5	
Length	L	12.000	m
Width	W	1.0000	
Height	H	0.6000	
Center of mass location	X_g	0.0120	m
	Y_g	0.000	
	Z_g	0.050	
Location of the center of buoyancy	X_b	0.000	N
	Y_b	0.00	
	Z_b	-0.025	

The position and direction of each thruster on the ROV, as presented in Table II, show the position coordinates and direction of each thruster.

$$\tau_x = \cos \alpha (u_3 + u_4 + u_7 + u_8)$$

$$\tau_y = \sin \alpha (u_3 - u_4 + u_7 - u_8) \sin \beta$$

$$\tau_z = \cos \beta (u_1 + u_2) + u_5 + u_6 + u_7 + u_8$$

$$\tau_\phi = 0.155 \cos \beta (u_1 - u_2) - 0.275 u_5 + 0.275 u_6 + 0.155 \cos \beta (u_7 - u_8)$$

$$\tau_\theta = 0.3945 \cos \beta (u_1 + u_2) + 0.4305 u_3 \cos \alpha (u_3 + u_4) - 0.0355 (u_5 + u_6) + 0.3945 (u_7 + u_8)$$

$$\tau_\psi = -0.3945 \sin \beta (u_1 - u_2) - 0.6605 \sin \alpha (u_3 - u_4) - 0.3945 (u_7 - u_8)$$

TABLE II. POSITION AND DIRECTION OF EACH THRUSTER ON THE ROV

Thruster	x_i	y_i	z_i	d_{xi}	d_{yi}	d_{zi}
T ₁	0.300	0.250	0.000	0.707	0.707	0.000
T ₂	0.300	-0.250	0.000	-0.707	0.707	0.000
T ₃	-0.300	-0.250	0.000	-0.707	-0.707	0.000
T ₄	-0.300	0.250	0.000	0.707	-0.707	0.000
T ₅	0.200	0.167	-0.200	0.000	0.000	-1.000
T ₆	0.200	-0.167	-0.200	0.000	0.000	-1.000
T ₇	-0.200	-0.167	-0.200	0.000	0.000	-1.000
T ₈	-0.200	0.167	-0.200	0.000	0.000	-1.000

The eight-thruster configuration consists of four horizontal thrusters (T₁–T₄) and four diagonal thrusters (T₅–T₈). This diagonal placement increases the arm moment, strengthens roll and pitch motion control, and improves vertical stability. In the 8-thruster configuration, T₅–T₈ are mounted diagonally at an angle θ (generally 45°) to the body axis. The force components in the XY plane originate from the projection and. For the force capability per axis of the diagonal thrusters to be equivalent to the reference thrusters aligned with the axis, a scale factor (k) was introduced in columns T₅–T₈. In this study, scale factor ($k = 1.2$) was chosen as a simple correction representing the combined effects of: the use of diagonal thruster pairs for XY-

plane maneuvers, the moment arm advantage, and flow efficiency in diagonal installation, as well as the equalization of maximum force rating per axis to the reference configuration. Thus, the projection components $k \cos \theta$ and $k \sin \theta$ are obtained, and their placement is depicted in Figure 2.

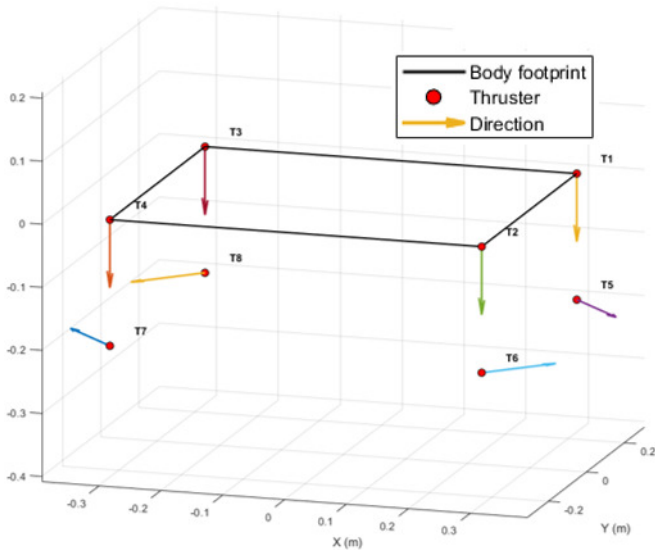


Fig. 2. Thruster placement on the ROV.

to stabilize the system without real-time feedback. Without a controller, the system oscillates or drifts, causing unwanted movement. To overcome this, the system can be linearized and given a controller, such as PID, to stabilize the position and orientation of the ROV and reduce oscillations.

Figure 3 illustrates the response of the nonlinear system to be controlled to test the response without feedback, which helps understand the dynamics of the system based on the specified parameters. This model entails a mass matrix (M) according to (5), which includes the total mass of the ROV and its components, as well as the moment of inertia used to calculate the force and torque generated by the thruster on each axis.

$$M = \begin{bmatrix} 95.392 & 0 & 0 & 0 & 0 & 0 \\ 0 & 128.435 & 0 & 0 & 0 & 0 \\ 0 & 0 & 201.144 & 0 & 0 & 0 \\ 0 & 0 & 0 & 5.312 & 0 & 0 \\ 0 & 0 & 0 & 0 & 17.083 & 0.010 \\ 0 & 0 & 0 & 0 & 0.010 & 6.993 \end{bmatrix}$$

This system also involves the damping matrix (D) in (10), which describes the resistance to movement, and the Coriolis matrix (C) in (6), which corrects for fictitious forces due to non-inertial motion. In addition, the gravitational force acting on the ROV is calculated using the G matrix in (12) to ensure that the gravitational force is handled according to the position and orientation of the ROV.

$$D = \begin{bmatrix} 5 & 0 & 0 & 0 & 0 & 0 \\ 0 & 20 & 0 & 0 & 0 & 0 \\ 0 & 0 & 20 & 0 & 0 & 0 \\ 0 & 0 & 0 & 2 & 0 & 0 \\ 0 & 0 & 0 & 0 & 10 & 0 \\ 0 & 0 & 0 & 0 & 0 & 10 \end{bmatrix}$$

$$C = \begin{bmatrix} 0 & 0 & 0 & 0 & 8.3072 & 0 \\ 0 & 0 & 0 & -8.3072 & 0 & 0.0604 \\ 0 & 0 & 0 & 0 & -0.0604 & 0 \\ 0 & 8.3072 & 0 & 0 & 0 & 0 \\ -8.3072 & 0 & 0.0604 & 0 & 0 & 0 \\ 0 & -0.0604 & 0 & 0 & 0 & 0 \end{bmatrix}$$

$$G = \begin{bmatrix} 0 & 0 & 0 & 0 & 0 & 0 \\ 0 & 0 & 0 & 0 & 0 & 0 \\ 0 & 0 & 0 & 0 & 0 & 0 \\ 0 & 0 & 0 & 7.848 & 0 & 0 \\ 0 & 0 & 0 & 0 & 7.848 & 0 \\ 0 & 0 & 0 & 0 & 0 & 0 \end{bmatrix}$$

The experimental results graph demonstrates that after applying RBFNN, the system exhibited significant improvements in both position and orientation stability, which were clearly observed on the X, Y, Z axes, as well as the Roll, Pitch, and Yaw orientations. Before the application of RBFNN, the system's position on the X axis oscillated between 0 and 2.5 m, indicating instability in horizontal position control. After RBFNN control was applied, these oscillations decreased dramatically, and the system moved more stably toward the setpoint value. Similarly, on the Y axis, the system exhibited stable oscillations around -1 m before the RBFNN was

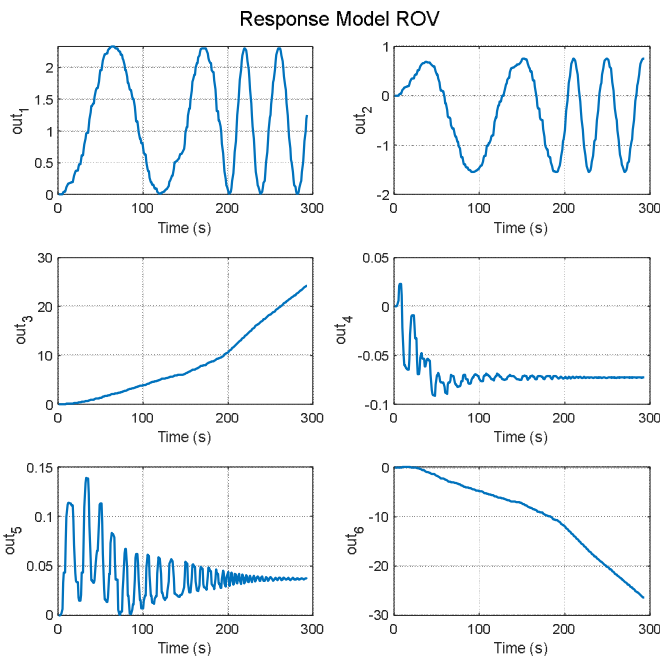


Fig. 3. ROV model response before control.

This matrix is used to calculate the thruster control required to generate torque on each axis so that the position and orientation of the ROV can be maintained as intended. However, without a controller, the ROV model response shows oscillations on several axes, such as the X axis (0–2.5 m), Y axis (approximately -1 m), and Z axis, which demonstrates uncontrolled movement. The applied thruster matrix is unable

implemented. After applying the control, the Y position began to approach the desired value in a more controlled manner, signifying an improvement in vertical position control. On the Z axis, which previously showed uncontrolled vertical drift, RBFNN was successful in stabilizing vertical movement, stopping any unwanted drift, and bringing the Z position to a stable point.

This experiment shows that RBFNN is effective in stabilizing position and reducing oscillations across all axes (X, Y, Z) and orientations (roll, pitch, yaw). The system's response became smoother, with more controlled and rapid movement toward the desired setpoint. This demonstrates that RBFNN not only helps reduce oscillations but also enhances the overall control precision of the system. Furthermore, the application of RBFNN, in combination with PID control, offers a more adaptive, stable, and responsive control system that can adjust to dynamic changes in system conditions.

An important factor in this improvement is the use of 8 thrusters in the ROV system. This configuration, with 4 horizontal thrusters and 4 diagonal thrusters, provides more robust control over the ROV's movement and orientation. The diagonal thrusters enhance stability and control, particularly in adjusting roll, pitch, and yaw, and also contribute to improved vertical movement control. By utilizing 8 thrusters, the ROV benefits from better maneuverability and stability in dynamic underwater conditions, making the RBFNN control system even more effective.

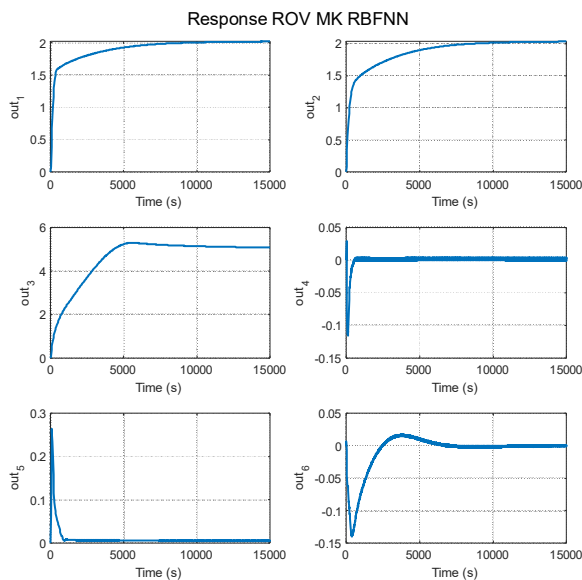


Fig. 4. ROV MK RBFNN response.

IV. CONCLUSION

This research successfully developed a control system for a Remotely Operated Vehicle (ROV) by utilizing Radial Basis Function Neural Network (RBFNN) to stabilize its position along the X, Y, and Z axes and its orientation in roll, pitch, and yaw. The experimental results show that after the application of RBFNN, the system experienced significant improvements in terms of stability, with oscillations on the X, Y, and Z axes

decreasing dramatically, and the position and orientation of the system became more stable and closer to the desired setpoint. Particularly on the Z axis, which previously showed drift, the application of RBFNN successfully stabilized vertical movement, and the roll, pitch, and yaw orientations also showed reduced oscillations with smoother and more controlled movements. RBFNN contributes significantly to dynamic control adjustment, allowing the system to move towards a stable condition more quickly without major deviations or oscillations, indicating that RBFNN not only reduces instability but also improves control precision. This RBFNN control system can overcome stability and responsiveness issues, making it more adaptive to changing conditions and improving overall system performance.

ACKNOWLEDGMENT

The authors express their gratitude to the Ministry of Higher Education, Science, and Technology for providing funding to carry out this research.

REFERENCES

- [1] K. Jothikrishna, S. M. Rithika, S. V. Swetha, and K. Kavitha, "Remotely Operated Underwater Vehicle (ROV)," in *2023 2nd International Conference on Advancements in Electrical, Electronics, Communication, Computing and Automation*, Coimbatore, India, June 2023, pp. 1–4, <https://doi.org/10.1109/ICAECA56562.2023.10200265>.
- [2] V. Venkatesh *et al.*, "Assessment of Structural Integrity of Submerged Concrete Structures Using Quantitative Non-Destructive Techniques Deployed from Remotely Operated Underwater Vehicles (ROV)," in *OCEANS 2022 - Chennai*, Chennai, India, Feb. 2022, pp. 1–6, <https://doi.org/10.1109/OCEANSChennai45887.2022.9775418>.
- [3] A. Kusumawardana, M. A. Habibi, L. Gumilar, and H. Purnata, "Reduction of Computational Burden on Observed Optimal Vector-Based FSMPC for SCIM Control fed 3L-NPC," *IAENG International Journal of Applied Mathematics*, vol. 55, no. 1, pp. 1–11, Mar. 2023.
- [4] H. Purnata, G. Aji, A. Musafiq, S. Rahmat, and A. Tafrikhatin, "Wind Energy Conversion System Using Finite Control Set Method: Predictive Control Model Connected to the Grid," in *Proceedings of the 5th International Conference on Applied Science and Technology on Engineering Science*, Bandung, Indonesia, 2022, pp. 358–365, <https://doi.org/10.5220/0011802900003575>.
- [5] J. Wen, J. Zhang, and G. Yu, "Predefined-Time Three-Dimensional Trajectory Tracking Control for Underactuated Autonomous Underwater Vehicles," *Applied Sciences*, vol. 15, no. 4, Feb. 2025, Art. no. 1698, <https://doi.org/10.3390/app15041698>.
- [6] H. Purnata, R. P. Dewi, S. Rahmat, E. Alimudin, and N. A. Ilahi, "Enhanced Depth Control and Stability in Submersible Pylon Inspection Robots Using IMU-Based Extended Kalman Filter and PID Control," *Jurnal Ecotipe (Electronic, Control, Telecommunication, Information, and Power Engineering)*, vol. 11, no. 2, pp. 224–234, Oct. 2024, <https://doi.org/10.33019/jurnalecotipe.v11i2.4523>.
- [7] Y. Wan, L. Xiao, and C. Wu, "A New Self-Adaptive Control Model and Application Basis on Optimum Fuzzy-RBFNN," in *2009 International Conference on Artificial Intelligence and Computational Intelligence*, Shanghai, China, 2009, pp. 582–585, <https://doi.org/10.1109/AICI.2009.144>.
- [8] T. T. K. Ly, N. T. Thanh, H. Thien, and T. Nguyen, "A Neural Network Controller Design for the Mecanum Wheel Mobile Robot," *Engineering, Technology & Applied Science Research*, vol. 13, no. 2, pp. 10541–10547, Apr. 2023, <https://doi.org/10.48084/etasr.5761>.
- [9] K. S. Arun Krishnan, J. Kadiyam, and S. Mohan, "Comparative Performance Investigations of the Intervention-class Underwater Vehicle With Different Possible Thruster Configurations Using Eight Identical Thrusters," *Ocean Engineering*, vol. 288, Nov. 2023, Art. no. 116147, <https://doi.org/10.1016/j.oceaneng.2023.116147>.

- [10] P. Krishnamoorthy, C. Tremblay, and P. Jackson, "Offshore Underwater Fixed Structure Integrity Assessment Using LRUT, PEC & ACFM Advanced Technologies with Minimal Marine Growth Removal," in *ADIPEC*, Abu Dhabi, UAE, Oct. 2023, Art. no. D031S089R006, <https://doi.org/10.2118/217037-MS>.
- [11] J. Jamieson, L. Wilson, W. Sherry, W. Main, and P. A. Solheimsnes, "The Underwater Intervention Drone, A New Method for Delivering IRM Services in the Subsea Environment," in *Offshore Technology Conference*, Houston, Texas, USA, Apr. 2018, Art. no. D011S009R003, <https://doi.org/10.4043/28766-MS>.
- [12] R. T. Hilmawan, "Penyelam Angkatan Laut Malaysia Tewas Tenggelam Saat Selamatkan Kapal Karam," *Kompas.com*, Kuala Lumpur, Malaysia, 29 Aug. 2024, <https://www.kompas.com/global/read/2024/08/29/113000270/penyelam-angkatan-laut-malaysia-tewas-tenggelam-saat-selamatkan-kapal>.
- [13] B. Chemisky, F. Menna, E. Nocerino, and P. Drap, "Underwater Survey for Oil and Gas Industry: A Review of Close Range Optical Methods," *Remote Sensing*, vol. 13, no. 14, July 2021, Art. no. 2789, <https://doi.org/10.3390/rs13142789>.
- [14] A. Gentili, F. Cagol, F. Ruscio, and R. Costanzi, "Comparison of Deep Learning Strategies for the Identification of Artificial Objects in Underwater Environment," in *OCEANS 2024 - Halifax*, Halifax, NS, Canada, Sep. 2024, pp. 1–6, <https://doi.org/10.1109/OCEANS55160.2024.10754484>.
- [15] Z. Kang, Z. Yuang, Y. Zhe, Z. Xiaoxin, W. Xinhui, and Q. Pengyuan, "Control Method for Posture Stabilization and Accurate Deployment of Remotely Operated Vehicles in Ocean Current Environments," in *Advances in Guidance, Navigation and Control*, vol. 1341, L. Yan, H. Duan, and Y. Deng, Eds. Singapore: Springer Nature Singapore, 2025, pp. 270–279.
- [16] M. B. Lubis, M. Kimiaei, and M. Efthymiou, "Alternative Configurations to Optimize Tension in the Umbilical of a Work Class ROV Performing Ultra-deep-water Operation," *Ocean Engineering*, vol. 225, Apr. 2021, Art. no. 108786, <https://doi.org/10.1016/j.oceaneng.2021.108786>.
- [17] M. Scerba, R. Sevcikova, S. Al-Rabeei, S. Mir, and N. Daneshjo, "Simulation Modeling of Kinematic Structures of Parallel Mechanisms," *Engineering, Technology & Applied Science Research*, vol. 15, no. 2, pp. 20714–20721, Apr. 2025, <https://doi.org/10.48084/etasr.9898>.
- [18] M. Jiang, C. Chen, Y. Dong, L. Zhang, and L. Tan, "Research on Hydrodynamic Characteristics and Dynamics Model of an Open-frame ROV Moving Near the Wall," *Ocean Engineering*, vol. 320, Mar. 2025, Art. no. 120358, <https://doi.org/10.1016/j.oceaneng.2025.120358>.
- [19] Y. Dai, C. S. Yang, X. Huang, and D. Xu, "RBF Neural Network Adaptive PID Control for Energy Storage System in Grid-Connected Photovoltaic Microgrid," in *2018 5th International Conference on Information, Cybernetics, and Computational Social Systems*, Hangzhou, China, Aug. 2018, pp. 212–217, <https://doi.org/10.1109/ICCSS.2018.8572478>.
- [20] X. H. Xia, and R. Yu, "Servo System PID Control of Neural Network Algorithm Based on Lure Model," *Chemical Engineering Transactions*, vol. 46, pp. 151–156, Dec. 2015, <https://doi.org/10.3303/CET1546026>.
- [21] X. Li, S. Duan, L. Wang, T. Huang, and Y. Chen, "Memristive Radial Basis Function Neural Network for Parameters Adjustment of PID Controller," in *Advances in Neural Networks – ISNN 2014*, vol. 8866, Z. Zeng, Y. Li, and I. King, Eds. Cham, Switzerland: Springer International Publishing, 2014, pp. 150–158.
- [22] X. Du, J. Wang, V. Jegatheesan, and G. Shi, "Dissolved Oxygen Control in Activated Sludge Process Using a Neural Network-Based Adaptive PID Algorithm," *Applied Sciences*, vol. 8, no. 2, Feb. 2018, Art. no. 261, <https://doi.org/10.3390/app8020261>.
- [23] S. M. Atif, S. Khan, I. Naseem, R. Togneri, and M. Bennamoun, "Multi-Kernel Fusion for RBF Neural Networks," *Neural Processing Letters*, vol. 55, no. 2, pp. 1045–1069, Apr. 2023, <https://doi.org/10.1007/s11063-022-10925-3>.
- [24] M. Zhang, W. Li, and M. Liu, "Adaptive PID Control Strategy Based on RBF Neural Network Identification," in *2005 International Conference on Neural Networks and Brain*, Beijing, China, 2005, vol. 3, pp. 1854–1857, <https://doi.org/10.1109/ICNNB.2005.1614987>.
- [25] C. S. Chin, W. P. Lin, and J. Y. Lin, "Experimental Validation of Open-frame ROV Model for Virtual Reality Simulation and Control," *Journal of Marine Science and Technology*, vol. 23, no. 2, pp. 267–287, June 2018, <https://doi.org/10.1007/s00773-017-0469-3>.